Consolidation of Combustion-Synthesized Titanium Diboride-Based Materials

Darren A. Hoke* and Marc A. Meyers*

University of California—San Diego, La Jolla, California   92093

The quasi-static consolidation in uniaxial compression of combustion-synthesized TiB$_2$-based materials was investigated. Consolidation was carried out in insulated containers upon completion of the combustion reaction, while the porous reaction products were ductile. Since the consolidation is not an isothermal process, the temperature change during consolidation was monitored and recorded. The effect of the addition of metallic elements to the elemental powders was established, and it was found that nickel and chromium provide the best compact integrity. The partial densification is sufficient to show significant differences between the effects of metallic additives. A phenomenological (not based on the micromechanisms of densification) constitutive model was applied to the hot and porous reaction products incorporating the temperature dependence of flow stress. The activation energy for the temperature dependence of the flow stress is established and indicates that, in addition to diffusion-induced plastic deformation, other processes occur, such as fracturing of ligaments.

I. Introduction

SELF-PROPAGATING high-temperature synthesis (SHS), reaction synthesis, and combustion synthesis all describe a unique method by which ceramics, intermetallics, and composites can be produced. The process involves the exothermic thermochemical reaction, either direct or indirect, of starting powders to form a product phase. The unique feature of the SHS process is that the combination reaction is self-sustaining until all of the reactants are converted to the product(s). The subject has been extensively reviewed by Munir and Anselmi-Tamburini[1] and Merzhanov.[2] Mechanisms of reaction synthesis have been reviewed by Munir[3] and Yi and Moore.[4] The energy released upon lowering the free energy of the starting materials to the product(s) typically raises the temperature of the product(s) to a point at which many contaminants (O, N, etc.) which may exist on the starting powders volatize, leaving behind escape paths in the freshly synthesized material. These escape paths, combined with a typical volume decrease during reaction and the initial porosity of the reacting mixture, produce a material with 40–50% residual porosity.

As-reacted materials can be crushed and used as abrasives or as high-purity powders for subsequent forming operations (e.g., sintering, hot-pressing, etc.). However, for general engineering applications most SHS-produced materials must undergo some type of postreaction processing to reduce residual porosity. Although significant work has proceeded with development of forced consolidation methods (hot pressing,[5–7] hot isostatic pressing,[8–10] explosive consolidation,[11–13] and hot forging[14–20]),

no systematic study on the mechanism(s) of forced consolidation is known to the authors. This study focuses on the forced consolidation of SHS-produced titanium diboride-based materials. Reaction temperatures are investigated as well as the effect of various metallic additives to help densification. A phenomenological (not based on the micromechanisms of deformation) constitutive equation which predicts the consolidation behavior and has a temperature dependence of flow stress, which is coupled with the measured temperature decay, is presented.

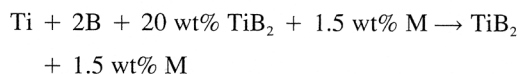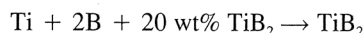## II. Materials and Methods

(1) Materials

High-purity (99.7%) titanium (Micron Metals, Inc., Salt Lake City, UT), 99.3% crystalline boron (Hermann C. Starck, Berlin, Germany), and 99.5% titanium diboride (Johnson-Matthey, Seabrook, NH) powders were dry mixed in polyethylene bottles with zirconia as a grinding medium for 24 h. To ensure that the final product composition fell within the region of the binary phase diagram where TiB$_2$ occurs, the titanium/boron powders were mixed in 33/67 at.% ratios. Presynthesized titanium diboride was added to the reactants as a diluent in order to obtain a well-controlled reaction suitable for postreaction processing; 1.5 wt% of several metallic elements—Ni (99.9%), Ta (99.9%) (Johnson Matthey, Seabrook, NH), Cr (99.9%), Hf (99.8%), and Mo (99.9%) (Cerac, Inc., Milwaukee, WI)—was added to one class of reaction to investigate their use as binders. All starting powders were −325 mesh, corresponding to particle sizes of less than 44 μm.

(2) Experimental Techniques

The following basic reaction was investigated:

$$Ti + 2B \rightarrow TiB_2$$
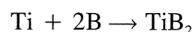
The addition of inert TiB$_2$ and metallic binder can be represented as

$$Ti + 2B + 20 \text{ wt\% TiB}_2 \rightarrow TiB_2$$

$$Ti + 2B + 20 \text{ wt\% TiB}_2 + 1.5 \text{ wt\% M} \rightarrow TiB_2$$
$$+ 1.5 \text{ wt\% M}$$

where M = Ni, Cr, Hf, Mo, Ta. These metallic elements were chosen specifically because they represent a range of melting points from a low of 1450°C (Ni), to a high of approximately 3000°C (Ta). It is also possible that some of these metals participate, to an extent, in the reaction. The mixed powders were uniaxially pressed into green compacts with a diameter of 31.8 mm, a height of 12.7 mm, and an approximate green density of 65–70% of theoretical.

The experimental configuration for reaction temperature measurement is shown schematically in Fig. 1; it is similar to the configuration used earlier by Dunmead *et al.*[21] The configuration consists of an enclosed reaction chamber in which the sample is placed and reacted, a data acquisition system to record and process thermocouple output voltage data, and a

---

variable transformer (Superior Electric Co., Bristol, CT) to facilitate remote ignition of the sample. Prior to ignition, the chamber was evacuated to approximately −0.8 atm and backfilled with argon gas to 1 atm. The samples were placed within insulated 49-mm-diameter steel rings to minimize heat losses during reaction. The insulation consisted of an Al_2O_3–Zr_2O_3 refractory board (Zircar Products Inc., Florida, NY) and was layered inside the steel ring with alumina cement (Zircar Products, Inc., Florida, NY) to yield a final inside diameter of approximately 31 mm. The assembly was vacuum cured for 24 h at 300°C and the inside diameter was bored out to approximately 31.9 mm.

Two 250-μm-diameter tungsten–5% rhenium vs tungsten–26% rhenium thermocouples (Omega Engineering, Stamford, CT) were inserted through preexisting holes drilled in the side of the steel ring such that they were positioned at the top and bottom surfaces of the sample. The average bead size of the thermocouples was 630 μm and the maximum service temperature was rated as 2316°C with short-term exposure up to approximately 2760°C. Data were collected over 60 s to adequately describe cooling of the product material(s). The entire steel ring fixture was sandwiched between two graphite plates to control expansion of the sample during reaction. Ignition of the sample was facilitated remotely from the top via ignition of approximately 5 g of a loose Ti + 2B powder mixture with an electrochemical match developed at UCSD.

An IBM PS/2 Model 25 computer equipped with a Metrabyte DAS-8 (Metrabyte, Corp., Taunton, MA) data acquisition board was utilized to monitor and collect the voltage output of the W–Re thermocouples. The system was configured to collect voltage data at a rate of 100 points/s from two separate channels.

(3) Compression Tests

The experimental configuration for the uniaxial compression tests consisted of 31.8 mm diameter by 12.7 mm high samples approximately 65–70% dense placed within insulated steel rings, identical to those used in the temperature measurement
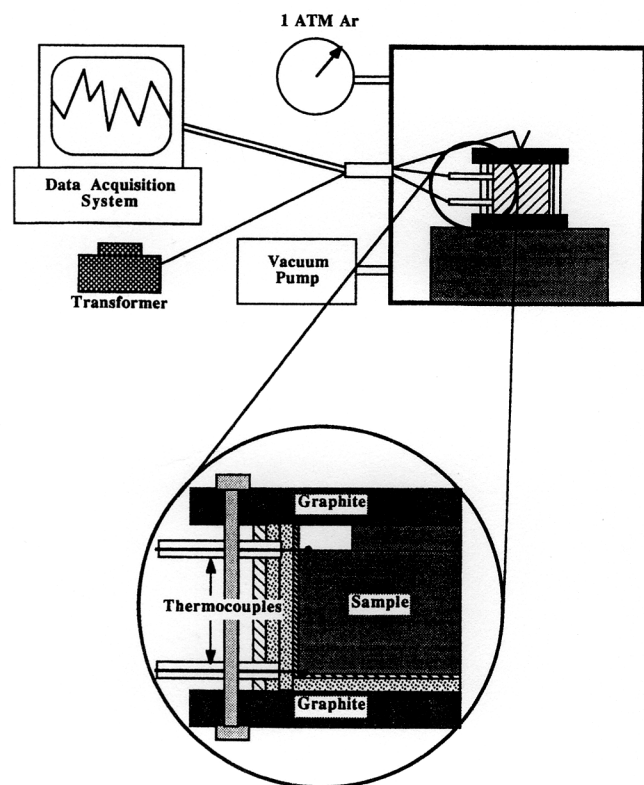
tests, and placed directly under the insulated ram of a modified Instron (Instron Corp., Canton, MA) uniaxial compression testing machine. The sample was remotely ignited via loose Ti + 2B powder, at which point, following complete synthesis, a load was applied at a constant rate of 5.1 cm/min to a maximum of 80 kN. Applied stress vs displacement data were sent to an X-Y chart recorder. Following compression, the samples were removed and allowed to cool within the insulated steel rings for subsequent sectioning and metallographic analysis.

III. Results and Discussion

(1) Synthesis of TiB$_2$

Figure 2 shows the as-reacted microstructure of SHS-produced TiB_2. The dark regions are large pores and the light gray regions are the SHS TiB_2. The formation of large pores within the as-reacted material is a result of the fact that the green compact has a high initial porosity; the sample undergoes a density increase upon formation of the product, and impurities expelled from the sample upon passage of the synthesis wave leave behind gas escape channels. The resultant porous skeletal structure consists of isolated regions of material approximately 50 μm in diameter connected by thin ligaments typically one or two grains wide (10–15 μm).

(2) Temperature Measurement

A typical experimentally determined temperature vs time profile for reaction-synthesized TiB_2 + 20% TiB_2 is shown in Fig. 3. Top and bottom thermocouple traces are represented by the solid and dashed lines, respectively. Several important features of these types of curves should be noted: (a) the reacted product(s) temperature generally drops below 1800°C within 10–15 s of ignition, (b) maximum reaction temperatures were not obtained from these tests because of breakup of the thermocouple signal at high temperatures, and (c) the top thermocouple trace consistently exhibited a higher temperature than the bottom thermocouple trace. These results are consistent with previous temperature measurements reported by Dunmead et al.[21] It should be noted that this experimental configuration measures only surface temperatures, which, due to heat losses to the surrounding insulation, cannot be assumed to represent bulk internal temperatures and are therefore presented as lower limits of the sample temperature.

Sample surface temperatures consistently dropped below 1800°C within 10–15 s of ignition for all the compositions examined and the resultant cooling curves exhibited a smooth exponential decay. These results are not consistent with those obtained by Kottke et al.,[22] who reported that 2-cm-diameter
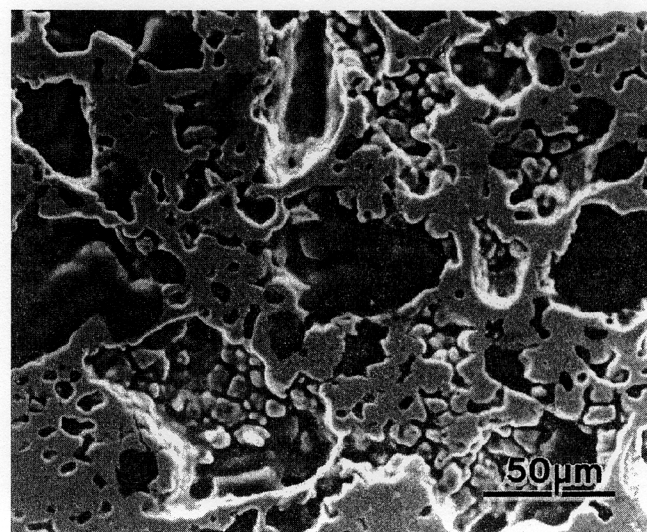

Fig. 1. Experimental configuration for temperature measurement tests illustrating sample containment and thermocouple placement.

Fig. 2. As-reacted microstructure of SHS-produced TiB$_2$.

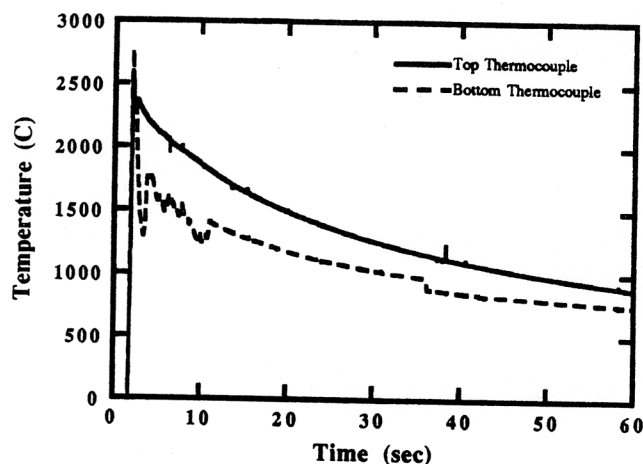**Fig. 3.** Experimentally determined temperature vs time profiles for reaction-synthesized TiB_2 with 20 wt% TiB_2 diluent.

Fig. 4. Enthalpy vs temperature data for Ti + 2B + 20 wt% TiB_2 and TiB_2 + 20 wt% TiB_2.[23]

SHS TiB_2 with 20 wt% TiB_2 diluent fell below 1800°C approximately 4 s after ignition. Their faster cooling rates are due to direct exposure to air.

Breakup of the thermocouple output signal during the early stages of the tests was a common feature and therefore maximum temperature measurement was not possible. The loss of signal is attributed to the melting of the thermocouple tips (W–5% Re vs W–26% Re alloys). The thermocouples (Type C) allow maximum service temperatures of 2316°C and short-term exposure up to 2760°C. Calculation of the maximum reaction temperatures can be done graphically by plotting both the reactant and product enthalpy vs temperature curves for a given composition. If one assumes all of the energy evolved from combination of the reactants to form the product goes into heating that product up to some temperature, then the point at which the product enthalpy equals that of the reactants (at the ignition temperature) will represent the maximum temperature of the reaction. The enthalpy vs temperature data for a number of elements can be found in Barin.[23] Enthalpy vs temperature data are plotted for Ti + 2B + 20% TiB_2 in Fig. 4. Assuming a heat of formation of 323.8 kJ/mol for TiB_2,[23] an adiabatic temperature of 3225°C is obtained. However, heat losses are always present and the adiabatic temperature is rarely achieved in actual experiments. These calculations indicate that the thermocouples may melt during synthesis, resulting in loss of signal. At some time later, when the sample temperature drops below the melting point of the W–Re alloy, the thermocouple signal is reacquired. This phenomenon was evident in all of the data collected.

Another interesting feature of these tests was the difference in measured temperature between the top and bottom thermocouples. The bottom thermocouple typically exhibited a lower temperature at a given time with respect to the top thermocouple. This is believed to be due to rapid heat conduction from the bottom surface of the sample to the insulation during reaction. Loss of heat to the bottom plate is represented by a decrease in surface temperature, at a given time, compared to that obtained from the top thermocouple.

In postreaction processing, cooling of the sample following synthesis is of more interest than the maximum temperature. Ramberg and Williams[24] reported plastic yielding in dense polycrystalline TiB_2 above 1800°C and this will be considered to be a ductile–brittle transition temperature, T_t, for TiB_2. From the data it can be seen that the samples typically drop below the transition temperature within 10–15 s of ignition; therefore, easiest consolidation should take place prior to this time. For larger samples, slower cooling rates are expected; therefore, these experiments give a lower bound over which a pressure, causing plastic deformation, can be applied before
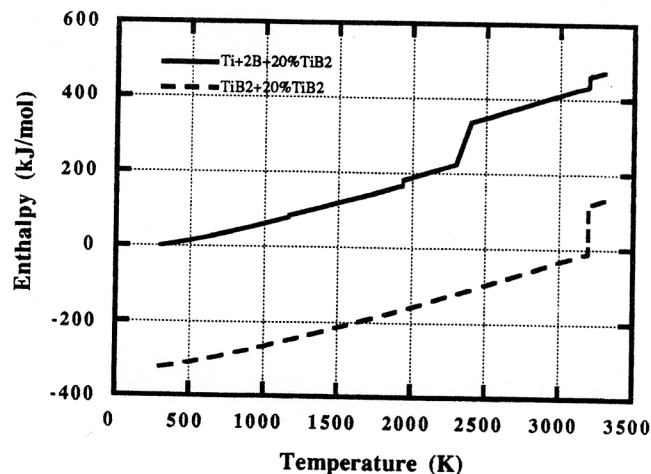
which the material reaches its critical ductile–brittle transition temperature.

Adding nickel to the SHS TiB_2 systematically decreased the reaction and postreaction temperatures as shown in Fig. 5. The top thermocouple traces are shown for 1.5, 5, and 10 wt% nickel over the first 14 s of the test. While the addition of 1.5 wt% Ni did not affect the reaction or postreaction temperature, the addition of 5 and 10 wt% Ni to the SHS TiB_2 resulted in a temperature drop below 1800°C within 9 and 4 s of ignition, respectively. The nickel acts as a heat sink during synthesis, lowering the reaction and postreaction temperatures to a point where consolidation may become difficult. The potentially detrimental loss of sample temperature is offset, however, by the fact that the nickel remains liquid until approximately 1500°C. Therefore, increasing the amount of nickel extends the time over which easy forced consolidation may occur even though sample temperatures may fall below the ductile transition temperature. The consolidation is helped, in this case, by the liquid nickel; however, Ni does not form a continuous phase at these low concentrations (1.5 and 5.0 wt%) and part of it may vaporize during the reaction (at 10% Ni, it will probably form a continuous phase filling the interstices between the synthesized TiB_2). Considering easy consolidation to occur above the melting point of nickel, it can be seen that the effective time for consolidation can be extended from approximately 5 to 11 s with the addition of 10 wt% Ni. Therefore, one must carefully consider the balance between postreaction temperature and binder fraction, since different consolidation mechanisms operate.
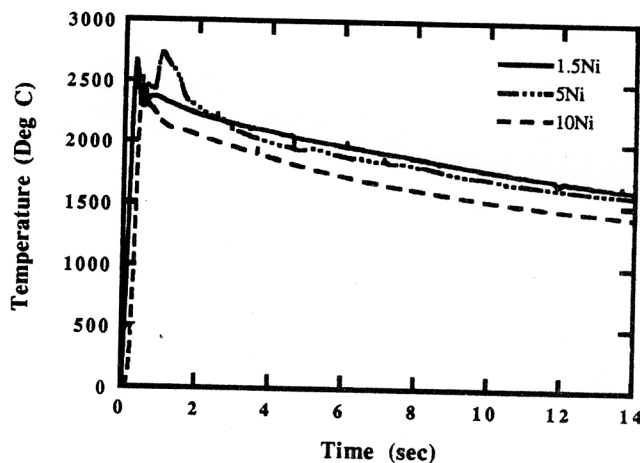

Fig. 5. Experimentally determined temperature vs time profiles for reaction-synthesized TiB_2 with 20 wt% TiB_2 diluent as a function of nickel content.

(3) Compression Test Results

Results from the uniaxial compression of the SHS TiB_2 and TiB_2 compositions containing 1.5 wt% M are shown in Fig. 6. Data are plotted as applied stress (MPa) vs relative density of the sample. Theoretical densities were calculated using the rule of mixtures for each composition. Direct combination of Ti and 2B exhibits a very stiff stress–density curve indicating little consolidation in the test configuration. At a compression rate of 5.1 cm/min a maximum sample density of 54% of theoretical was achieved under an applied stress of 110 MPa. With the addition of 20 wt% TiB_2 diluent the curves translated to the right, resulting in greater consolidation (65% of theoretical) for the same applied stress. Further increases in sample density were also evident for some of the binders; the best results were obtained with the lower melting point elements (e.g., Ni, Cr). Maximum densities of 68% of theoretical were obtained with Ni as the binder phase. It should be emphasized that the objective of these experiments was not to fully densify the reaction products, but to establish their response to applied compressive stresses at high temperatures. The maximum operating load of the testing machine (80 kN) is insufficient to generate the stresses required to completely collapse the voids; for instance the DYNAPAK[14] or CERACON[25] processes apply much higher specific energies to the compacts and yield fully dense (>97% theoretical) compacts.

Figure 7 shows the macrostructural integrity of the compressed samples with the loading direction indicated by arrows. As expected from the experimental data, the Ti + 2B sample exhibits the poorest overall integrity while the compositions containing diluent and binder (especially, Ni) exhibit the best integrity. The diluent acts as a moderator to the violent elemental reaction decreasing the velocity of the synthesis wave, resulting in a more controlled reaction with slower removal of powder contaminants. Thermodynamic analysis indicates that the adiabatic temperature remains constant with the addition of 20 wt% diluent; however, the end result is a higher integrity, lower porosity sample. Kottke et al.[22] reported similar results in their study of the effect of inert dilutions and mechanical restraint on the integrity of SHS-produced TiB_2: moderate additions of TiB_2 diluent reduced propagation rates and sample loss during synthesis, thereby enhancing postreaction sample integrity.

Microstructures of some of the compacted samples are shown in Figs. 8–10 with the load direction indicated. The microstructure of the compressed Ti + 2B sample, Fig. 8, consists of a rigid cellular block-type structure with no evidence of postsynthesis deformation. This is an interesting result, given the high temperature of the reaction ($T_{ad} \approx 3200°C$). Apparently, the sample cooled so fast following synthesis that the initial skeletal structure was maintained and able to resist the

applied stress of 110 MPa. Comparing the Ti + 2B sample to the sample containing 20 wt% TiB_2, Fig. 9(a), reveals a much finer granular-type microstructure consisting of packed particles on the order of 10–20 μm in diameter. This microstructure results from the crushing of the initial SHS structure (Fig. 2) into small particles under the applied load. The particles do not show evidence of extensive plastic deformation perpendicular to the load axis; however, there is evidence of rounding of particle surfaces and interparticle necking, Fig. 9(b) (arrow A), as a result of the high temperatures.

Addition of 1.5 wt% Ni and Cr to the TiB_2 improved the overall integrity of the samples and enhanced interparticle bonding. The material containing diluent but no binder exhibited an apparent mechanical interlocking of particles following compression while evidence of greater interparticle necking and better particle bonding was evident with the addition of 1.5 wt% Ni and Cr. A backscattered electron micrograph (Fig. 10) revealed that the nickel binder resided at the grain boundary (arrow A) and interparticle interfaces (arrow B). The composition containing 1.5 wt% Cr showed similar results. This is consistent with results reported earlier.[14] The microstructures of the materials containing Hf, Mo, and Ta were also characterized. These materials exhibited granular-type microstructures similar to the material containing only diluent with no evidence of enhanced bonding or wetting of the TiB_2 grains. Whereas there was no evidence that Mo and Ta reacted with Ti-B, Hf showed a graded intensity distribution in backscattered SEM images, indicating possible solubility. In Table I, it can be seen that Hf has an HCP structure, which would facilitate the possibility of solubility in TiB_2.

Table I lists some of the important characteristics of the binder materials. As mentioned earlier, these elements were chosen specifically because they represent a wide range of melting temperatures. If an adiabatic reaction temperature of 3200°C is assumed, all the binders are expected to melt upon passage of the reaction wave through the sample. However, for the binder to be effective in providing lubrication for grain boundary sliding during compression, and to enhance grain boundary diffusion after compression, it should remain a liquid phase as long as possible. According to the cooling curves, the high melting point materials, Ta (3014°C) and Mo (2617°C), will exist as a liquid phase for only a very short time (1–2 s) after which they will transform into ductile then hard inclusions, possibly hindering forced consolidation efforts. This is evident in Fig. 11; the microstructure of the sample containing 1.5% Ta looks identical to the material containing no binder (Fig. 9). By lowering the melting point of the binder, the time over which the material can aid the densification (as long as the material wets the TiB_2) is effectively extended.

Figure 12 shows the effect of increasing nickel content on the compression behavior of SHS TiB_2. As the amount of nickel increases, the material becomes easier to consolidate, as shown by translation of the stress vs density curves to the right. Maximum relative densities of 68% and 73% of theoretical were obtained with the addition of 5 and 10 wt% nickel, respectively. Increases in relative density for similar applied loads confirm that the potentially detrimental loss of sample temperature is offset by the increased fraction of nickel binder which remained as a liquid over the period of the test.

Microstructures of the compressed SHS TiB_2 with 1.5%, 5%, and 10% Ni are shown in Fig. 13. At low nickel concentrations (1.5 wt%), the binder resides as a thin layer coating the grain boundary interfaces (arrow A), Fig. 13(b). As the amount of nickel increases (5 wt%), it becomes distributed as both thin layers (arrow A) and clumps (arrow B), Fig. 13(d). Larger amounts of nickel (10 wt%) reveal regions of entire grains surrounded by the binder, Fig. 13(f).

(4) Modeling of Densification Behavior

Prediction and understanding of the consolidation behavior of SHS-produced materials is a necessary step in the evolution of reaction synthesis from the laboratory to industry. Numerous
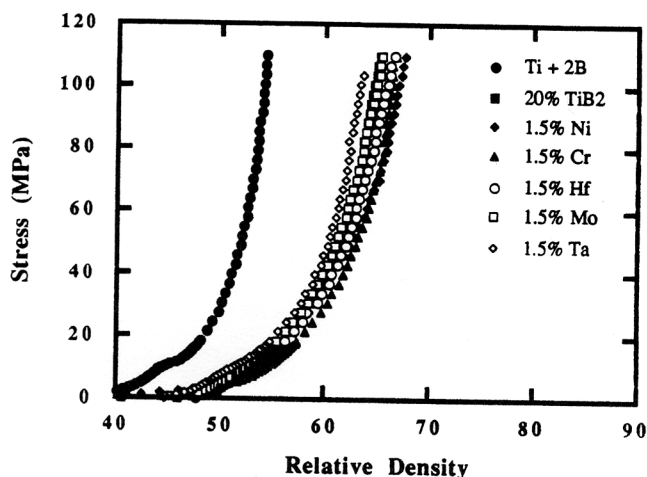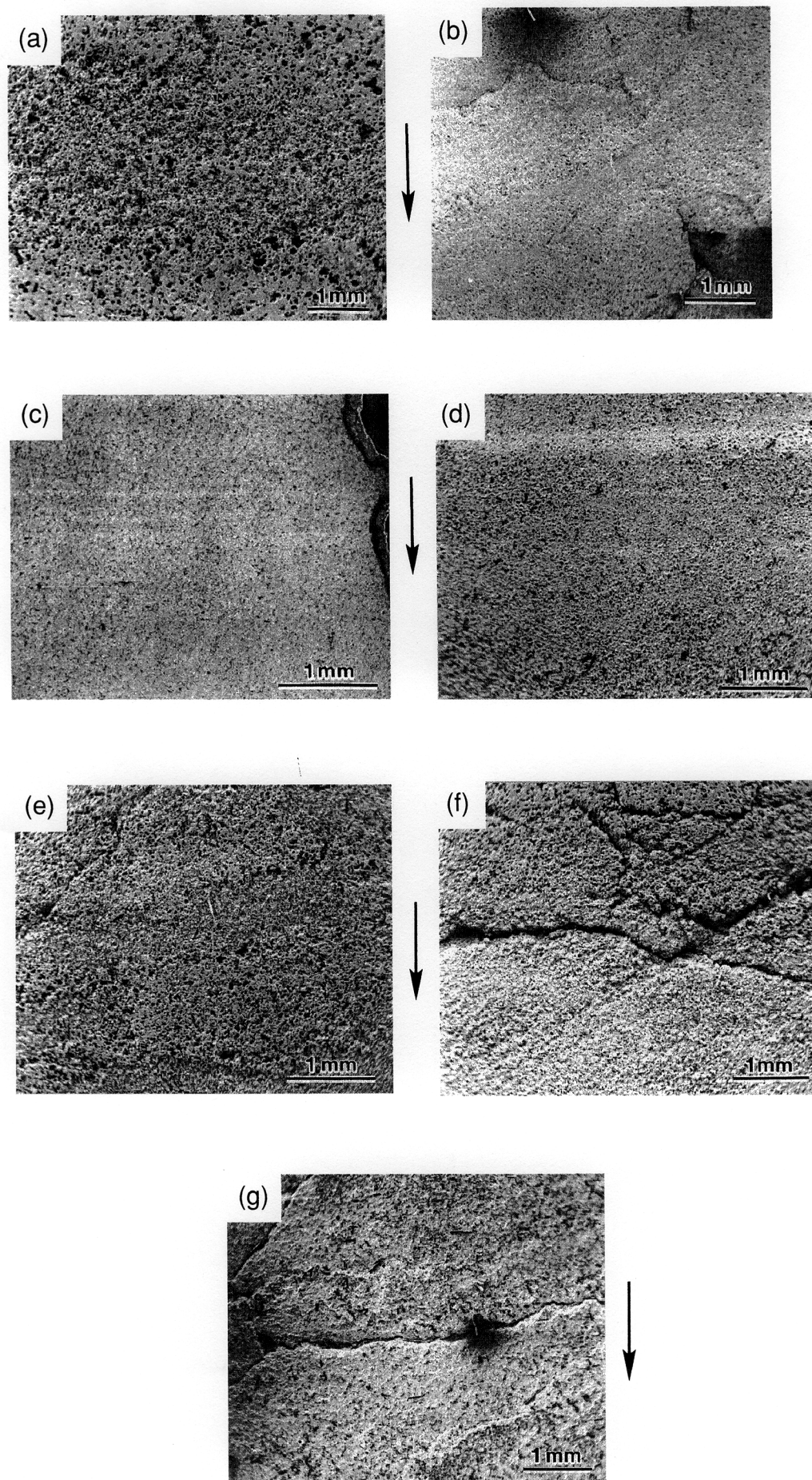
Fig. 6. Stress vs relative density for the uniaxial compression of SHS TiB_2 with 1.5 wt% M.

Fig. 7. Macrostructural integrity of compressed SHS samples: (a) Ti + 2B, (b) 20 wt% TiB_2, (c) 1.5% Ni, (d) 1.5% Cr, (e) 1.5% Hf, (f) 1.5% Mo, (g) 1.5% Ta.
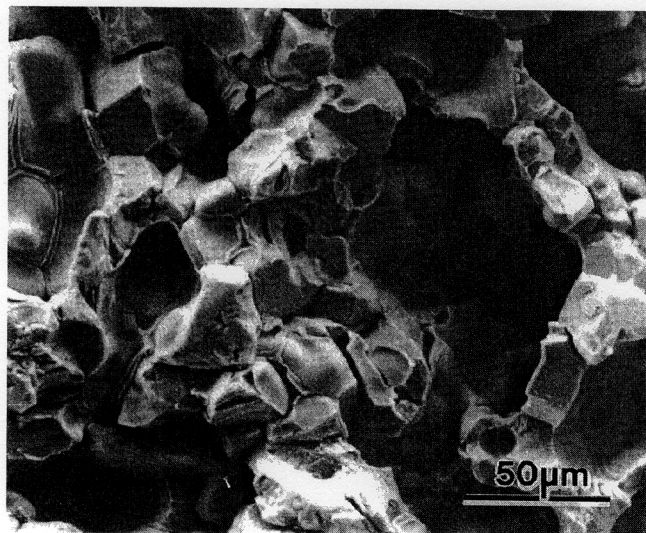
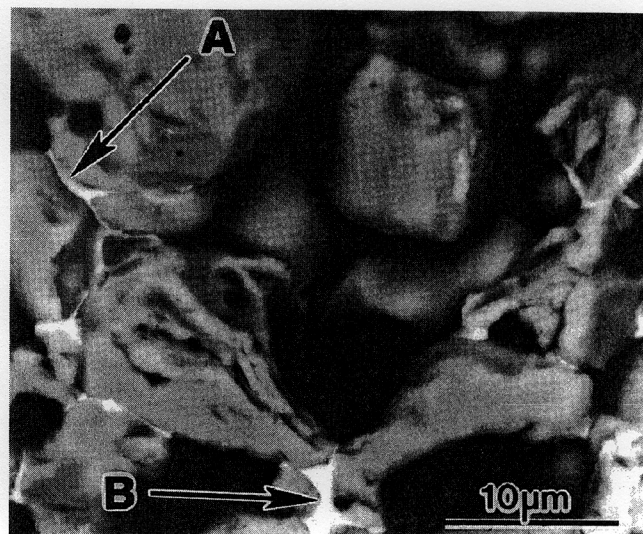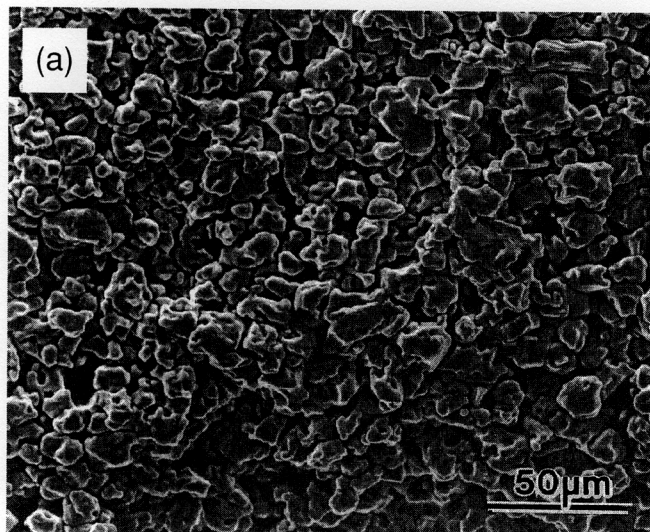**Fig. 8.** Microstructure of compressed SHS Ti + 2B.

Fig. 10. Microstructure of compressed SHS TiB_2 with 1.5% Ni; backscattered image showing nickel residing at grain boundaries (arrow A), and interparticle interfaces (arrow B).

constitutive equations for porous and granular materials have been developed, and they basically fall into two categories: (a) plasticity (phenomenological) equations and (b) microstructurally based equations. Constitutive equations based on simple void collapse mechanisms have been proposed, for instance, by Green,[26] Carrol and Holt,[27] and Banks-Sills and Budiansky.[28] Models incorporating more realistic depictions of powders were developed by Helle *et al.*,[29] Oyane *et al.*,[30] and McMeeking and co-workers.[31,32] The reaction synthesis products under investigation exhibit a very complex microstructure, and it was not felt appropriate to use a constitutive model based on plastic deformation of spheres, such as Heller *et al*'s.[29] and McMeeking's[31] models. Therefore, the "engineering" model proposed by Kuhn and Downey,[33] and extended by Doraivelu *et al.*,[34] was applied to the data. There is no assumption of a homogeneous material, and the form of the equation is obtained empirically from observed behavior.

Plastic deformation of porous materials is described by the von Mises (J_2) criterion modified to incorporate the effect of the hydrostatic component of stress, I_1. For isothermal conditions yielding in a ductile porous material, Kuhn and Downey[33] proposed the following expression:

$$\delta Y_0^2 = AJ_2 + BI_1^2 \tag{1}$$

Table I. Basic Physical Characteristics of Binder Materials

	Atomic number	Crystal structure	Melting point (°C)	Boiling point (°C)	Density (g/cm³)
Nickel	28	FCC	1453	2914	8.9
Chromium	24	BCC	1857	2672	7.19
Hafnium	72	HCP	2227	4603	13.3
Molybdenum	42	BCC	2617	4639	10.2
Tantalum	73	BCC	3014	5458	16.6

where Y_0 is the flow stress of the fully dense material, I_1 is the first invariant of the stress tensor, and J_2 is the second invariant of the deviatoric stress; various expressions have been proposed for A, B, and δ. Kuhn and Downey[33] proposed expressions for A, B, and δ, in terms of the relative density of the body; $A = (2 + R^2)$, $B = (1 - R^2)/3$, and $\delta = 1$, where R is the relative density of the sample (equal to the ratio between actual and theoretical density). For the case of uniaxial strain compression of cylindrical bodies, the lateral stresses can be expressed as
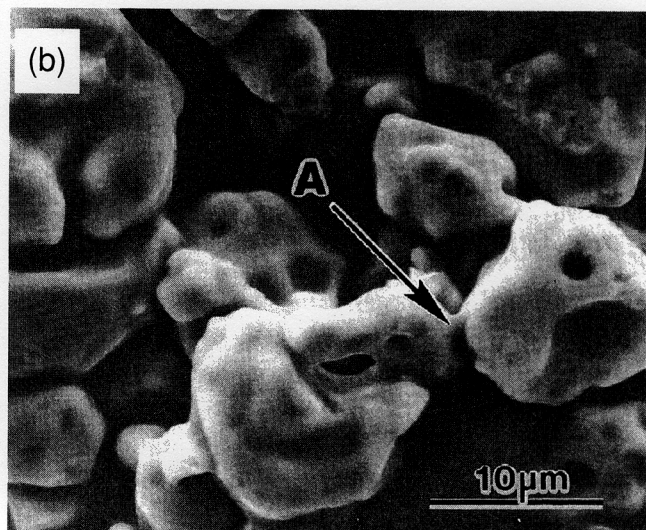

Fig. 9. Microstructure of compressed SHS TiB_2 with 20% TiB_2: (a) low magnification, (b) high magnification illustrating postcompaction interparticle necking (arrow A).
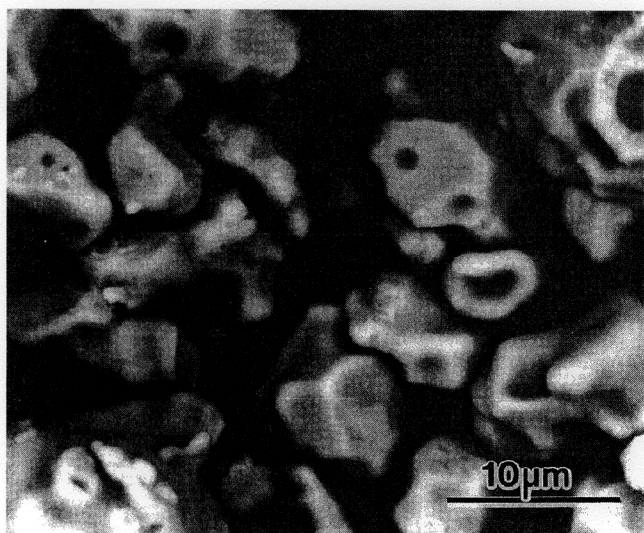
Fig. 11. Microstructure of compressed SHS TiB$_2$ with 1.5% Ta; backscattered electron image illustrating relatively no compaction along the load axis.
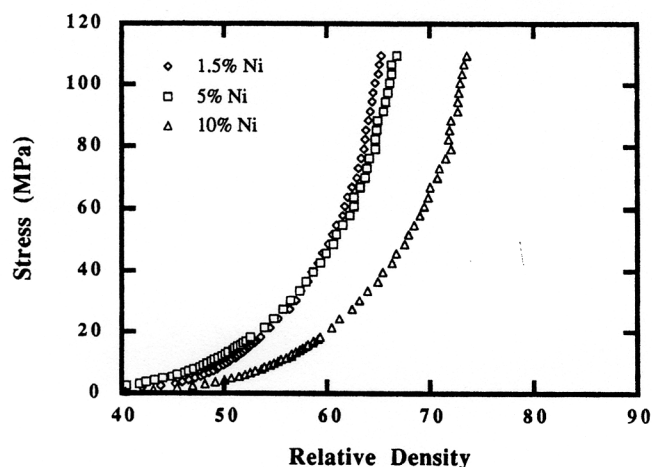

Fig. 12. Stress vs relative density for uniaxial compression of SHS TiB$_2$ as a function of nickel content.

$$\sigma_r = \sigma_\theta = \left[\frac{R^2}{(2 - R^2)}\right]\sigma_z \tag{2}$$

$$I_1 = \sigma_r + \sigma_\theta + \sigma_z = \left[\frac{(R^2 + 2)}{(2 - R^2)}\right]\sigma_z \tag{3}$$

$$J_2 = \frac{1}{6}[(\sigma_r + \sigma_\theta) + (\sigma_\theta + \sigma_z) + (\sigma_z + \sigma_r)]$$

$$= \frac{1}{3}\left[\frac{(1 - R^2)}{(2 - R^2)}\right]^2\sigma_z^2 \tag{4}$$

Solving Eq. (1) for the applied stress σ_z, the yield criterion is given by

$$\sigma_z = Y_0\left[\frac{(2 - R^2)}{(1 - R^2)(2 + R^2)}\right]^{0.5} \tag{5}$$

Doraivelu *et al.*[34] further modified Eq. (5) by assuming a dependence of the yield stress on the relative density of the form

$$\delta = \frac{R^2 - R_c^2}{1 - R_c^2} \tag{6}$$

where R_c is the critical density at which we assume the material

to lose all mechanical strength. This enables resistance of the material to compression to rise gradually from zero. Equation (5) takes the form

$$\sigma_z = Y_0\left[\frac{R^2 - R_c^2}{1 - R_c^2}\right]^{0.5}\left[\frac{(2 - R^2)}{(1 - R^2)(2 + R^2)}\right]^{0.5} \tag{7}$$

Equation (7) is valid for isothermal conditions; however, temperature drops significantly over the duration of the test in the experiments conducted on the reaction synthesis products. A simple and realistic representation of the yield stress variation with temperature is given by an Arrhenius relationship:

$$Y(T) = Y_0\exp\left[\frac{Q}{KT(t)}\right] \tag{8}$$

where Y_0 is the flow stress of the fully dense material at a reference temperature T_0, K is Boltzmann's constant, $T(t)$ is the temperature of the sample (function of time), and Q is the apparent activation energy for deformation.

Figure 14 shows the flow stress, Y_0, of the SHS TiB$_2$–20% TiB$_2$ plotted as a function of temperature for a typical compression test; the values for Y_0 are obtained from the experimental results of Fig. 6. The temperature of the sample during compression is assumed to be identical to that in the temperature measurement tests. This assumption is not strictly correct if we consider that the sample density changes over the period of the test, increasing the thermal conductivity of the sample whereas the temperature measurements were made on the porous material. Assuming the cooling rate to be the same for both cases, it is seen that the flow stress does, in fact, show an exponential dependence with temperature. Normalizing the temperature dependence of the yield stress against an assumed transition temperature, above which plastic deformation is expected to occur, $T_t = 1800°C$, one can modify Eq. (8):

$$Y(T) = Y_0\exp\left[\frac{Q}{K}\left(\frac{T - T_t}{TT_t}\right)\right] \tag{9}$$

By incorporating Eq. (9) into Eq. (7), the flow stress of hot, porous, as-synthesized SHS materials is given by

$$\sigma_z = Y_0\exp\left[\frac{Q}{K}\left(\frac{T - T_t}{TT_t}\right)\right]\left[\frac{R^2 - R_c^2}{1 - R^2}\right]^{0.5}$$

$$\times \left[\frac{(2 - R^2)}{(1 - R^2)(2 + R^2)}\right]^{0.5} \tag{10}$$

From the compression tests R_c, R, T, and T_t are directly determined. Values for Y_0 and Q can be calculated to best fit the experimentally determined data; this is shown in Fig. 15, where both the model and experiment are represented for the compression of Ti + 2B + 20% TiB$_2$. Good agreement is obtained between the model and experiment for all compositions investigated.

Table II lists the calculated flow stresses, Y_0, and apparent activation energies, Q, for Ti + 2B, Ti + 2B + 20 wt% TiB$_2$, and each of the compositions containing 1.5 wt% M; the effect of Ni is also shown. The calculated flow stress, Y_0, varied between the seven compositions from a low of 90 MPa (Cr and Mo) to a high of 400 MPa (Hf); the apparent activation energy for deformation, Q, was taken as 289.0 kJ·mol^{-1} for these compositions. The value of Y_0 that best fits the experimental data is somewhat artificial because it is based on a reference temperature of 1800°C. Yielding of hot-pressed TiB$_2$ (12 μm grain size) at 1800°C has been reported at stresses of approximately 480–500 MPa.[24] Thus, the values of Y_0 predicted through Eq. (10) are reasonable and comparable to those obtained from actual compression tests on hot-pressed TiB$_2$.

By plotting log σ_z vs $1/T$ in an Arrhenius plot, the apparent activation energy for deformation can be determined. Figure 16 shows this plot of experimentally determined stress–temperature data for SHS and hot-pressed[24] TiB$_2$. Apparent activation
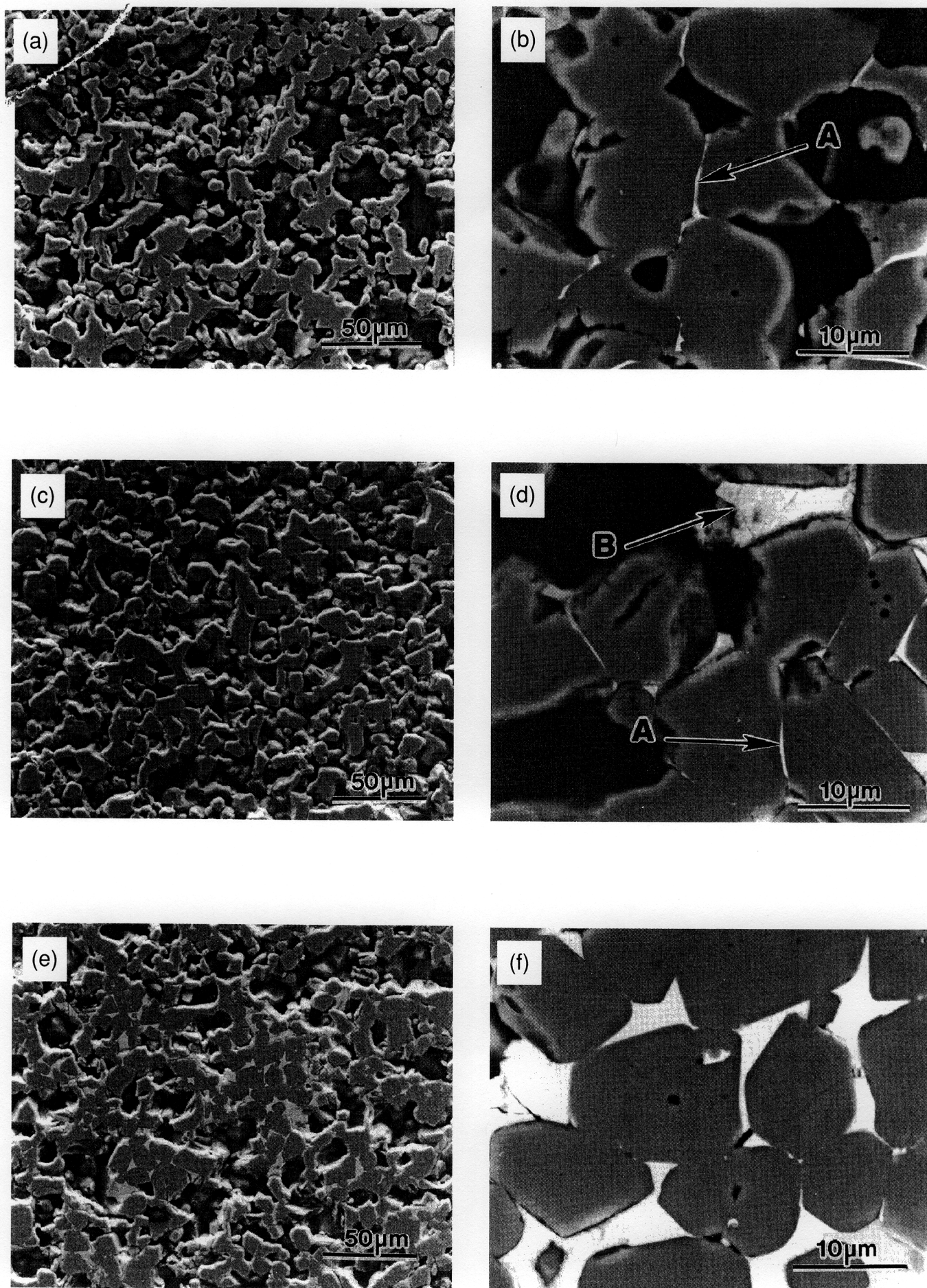
Fig. 13. Backscattered electron micrographs of compressed TiB$_2$: (a,b) 1.5% Ni, (c,d) 5% Ni, and (e,f) 10% Ni.
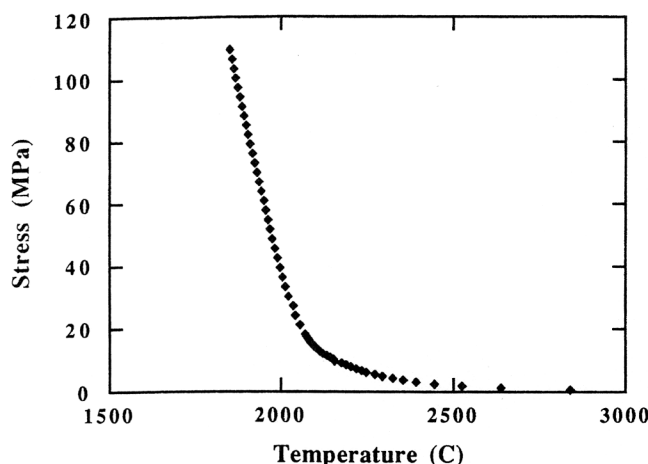
Fig. 14. Experimentally determined flow stress vs temperature for SHS TiB_2 with 20 wt% TiB_2 diluent.
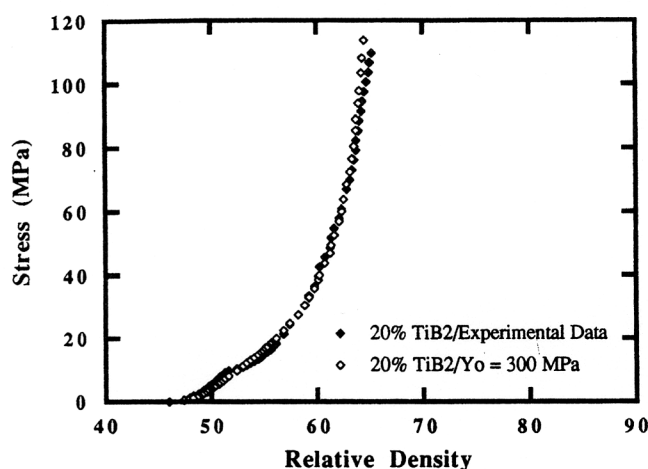

Fig. 15. Comparison of the constitutive model and experimental data for the uniaxial compression of hot as-reacted TiB_2 with 20 wt% TiB_2 diluent.

Table II. Calculated Flow Stress at Reference Temperature of 1800°C, Y_0 (MPa), and Apparent Activation Energies, Q (kJ·mol^{-1})

	Y_0 (MPa)	Q (kJ·mol^{-1})
Effect of inert TiB_2 and metallic binder		
TiB_2	160	289.0
TiB_2 + 20% TiB_2	300	289.0
TiB_2 + 20% TiB_2 + 1.5% Ni	130	289.0
TiB_2 + 20% TiB_2 + 1.5% Cr	90	289.0
TiB_2 + 20% TiB_2 + 1.5% Hf	400	289.0
TiB_2 + 20% TiB_2 + 1.5% Mo	90	289.0
TiB_2 + 20% TiB_2 + 1.5% Ta	340	289.0
Effect of Ni content		
TiB_2 + 20% TiB_2 + 1.5% Ni	130	289.0
TiB_2 + 20% TiB_2 + 5% Ni	20	240.8
TiB_2 + 20% TiB_2 + 10% Ni	9	240.8

energies of 366.0 kJ·mol^{-1} for the SHS TiB_2, and 67.5 kJ·mol^{-1} for the hot-pressed TiB_2, are calculated from the data. However, to obtain a value for the true activation energy for plastic deformation, E, Ramberg and Williams[24] proposed that the apparent activation energy, Q, calculated from the slope of the Arrhenius plot of log σ_z vs $1/T$, must be multiplied by the factor $n + 2$, where n is the stress exponent obtained from dead-load experiments. Assuming a value of $n = 2$, true activation energies for
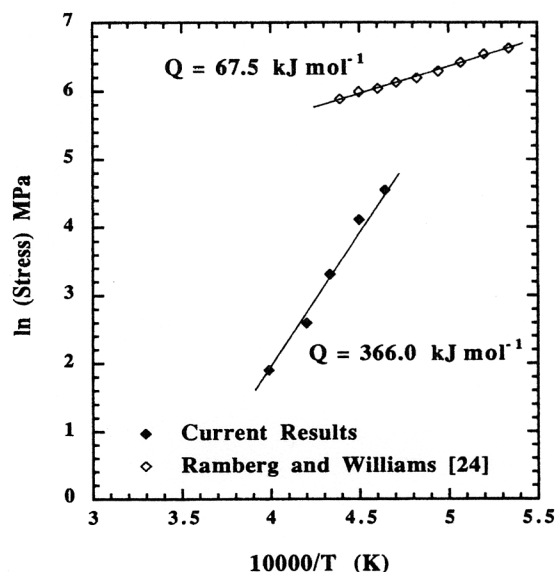

Fig. 16. Arrhenius plot of flow stress vs $1/T$ for SHS and hot-pressed TiB_2.[24]

plastic deformation of 1464.1 and 269.7 kJ·mol^{-1} are calculated for the SHS and hot-pressed TiB_2, respectively.

Differences between the activation energies and temperature dependences obtained for the SHS specimens in the current research (through Eq. (10)) and the results obtained by Ramberg and Williams[24] can be attributed to fundamental differences in the deformation mechanisms. If the collapse of porosity were accomplished exclusively by plastic deformation, the data should superimpose, assuming that the constitutive equation (Eq. (10)) is correct. Therefore, it is clear that an additional deformation mechanism, such as breakup of the skeletal structure (fracture) is operative. Indeed, Figs. 8 and 9 show how the particles are fractured during compression. The fracturing of a skeletal structure under imposed compression is necessarily a process with a different activation energy. An additional factor is the presence of a metallic phase (Ni) which is liquid during the densification process. Particle rearrangement, which would be aided by a liquid phase, would contribute to a process with different activation energy, because it is controlled by interparticle friction which, in turn, is highly dependent on the presence of a liquid phase acting as a lubricant.

Figure 17 shows the excellent correlation between model and experiment for the samples containing 5 and 10 wt% nickel. Table II lists the calculated flow stress and apparent activation energies for the samples containing nickel. The calculated flow stress and apparent activation energy decrease with increasing nickel content. Calculated flow stress is reduced from 130 MPa (1.5% Ni) to 20 MPa (5% Ni) to 9 MPa (10% Ni). A 97% decrease in the energy required for the consolidation of TiB_2 + 20% TiB_2 is achieved with the addition of 10 wt% nickel. The corresponding decrease in activation energy from 289.0 kJ·mol^{-1} (1.5% Ni) to 240.8 kJ·mol^{-1} (5% and 10% Ni) also suggests that the mechanism of consolidation changes from breakup of the skeletal structure to some type of easier consolidation mechanism, perhaps via grain boundary sliding.

IV. Conclusions

The effect of various metallic elements as potential densification aids in reaction-synthesized titanium diboride were investigated through instrumented partial consolidation experiments and a mechanical analysis. Low melting point binders (Ni, Cr) provided the best consolidation due to the fact that they remained a liquid phase for a longer time than the high melting point materials. Of the binders investigated, Ni, Cr, Hf, Mo, and Ta all remain as a second phase, residing at grain boundaries
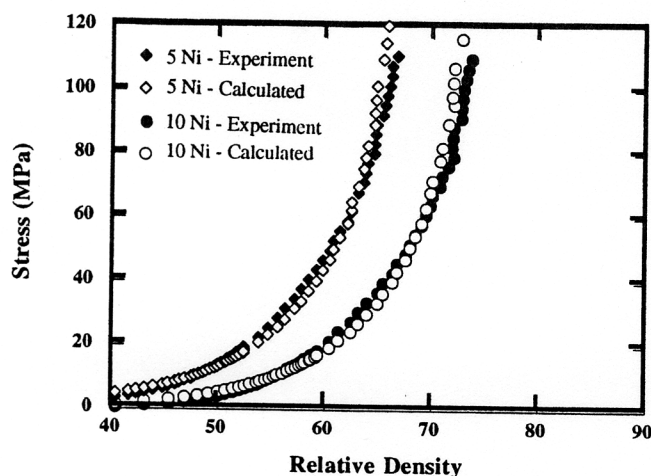
Fig. 17. Comparison of the constitutive model and experimental data for the uniaxial compression of hot as-reacted TiB_2 with 20 wt% TiB_2 diluent and 5.0 and 10.0 wt% Ni.

and interparticle interfaces with the exception of hafnium which appeared to form a solid solution with the TiB_2. Increases in the amount of nickel resulted in further increases in consolidation. These results indicate the following:

(a) Forced consolidation techniques which occur over small time scales such as high-speed forging may be preferable over techniques which require substantially more time such as hot-pressing or hot isostatic pressing.

(b) Insulation of the sample during and after synthesis is important.

(c) Binder composition and fraction are important.

(d) A simple constitutive equation has been developed which accurately describes the consolidation behavior of SHS-produced materials. Apparent activation energies of 366 $kJ \cdot mol^{-1}$ were calculated for the plastic deformation of SHS TiB_2 containing 20 wt% TiB_2 diluent.

References

[1]Z. A. Munir and U. Anselmi-Tamburini, "Self-Propagating Exothermic Reactions: The Synthesis of High-Temperature Materials by Combustion," _Mater. Sci. Rep._, **3**, 281–365 (1989).

[2]A. G. Merzhanov; p. 1 in _Combustion and Plasma Synthesis of High Temperature Materials_. Edited by Z. A. Munir and J. B. Holt. VCH Publishers, New York, 1990.

[3]Z. A. Munir, "Reaction Synthesis Processes: Mechanisms and Characteristics," _Metall. Trans._, **23A**, 7–13 (1992).

[4]H. C. Yi and J. J. Moore, "Review: Self-Propagating High-Temperature (Combustion) Synthesis (SHS) of Powder-Compacted Materials," _J. Mater. Sci._, **25**, 1159–68 (1990).

[5]J. B. Holt and Z. A. Munir, "Combustion Synthesis of Titanium Carbide: Theory and Experiment," _J. Mater. Sci._, **21**, 251–59 (1986).

[6]G. Y. Richardson, R. W. Rice, W. J. McDonough, J. M. Kunetz, and T. Schroeter, "Hot Pressing of Ceramics Using Self-Propagating Synthesis," _Ceram. Eng. Sci. Proc._, **7**, 761–70 (1986).

[7]M. A. Riley and A. Niiler, "Low Pressure Compaction of SHS Prepared Ceramics," Report No. BRL-MR-3574, Ballistic Research Laboratory, U.S. Army Laboratory Command, Aberdeen Proving Ground, Maryland, March 1987, pp. 1–21.

[8]Y. Miyamoto, K. Koizumi, and O. Yamada, "High-Pressure Self-Combustion Sintering for Ceramics," _J. Am. Ceram. Soc._, **67** [11] C-224–C-225 (1984).

[9]O. Yamada, Y. Miyamoto, and M. Koizumi, "High-Pressure Self-Combustion Sintering of Silicon Carbide," _Am. Ceram. Soc. Bull._, **64** [2] 319–21 (1985).

[10]S. Adachi, T. Wada, T. Michara, Y. Miyamoto, and M. Koizumi, "High-Pressure Self-Combustion Sintering of Alumina–Titanium Carbide Ceramic Composite," _J. Am. Ceram. Soc._, **73** [5] 1451–52 (1990).

[11]L. J. Kecskes, R. F. Benck, and P. H. Netherwood, Jr., "Dynamic Compaction of Combustion-Synthesized Hafnium Carbide," _J. Am. Ceram. Soc._, **73** [2] 383–87 (1990).

[12]L. J. Kecskes, T. Kottke, and A. Niiler, "Microstructural Properties of Combustion Synthesized and Dynamically Consolidated Titanium Boride and Titanium Carbide," _J. Am. Ceram. Soc._, **73** [5] 1274–82 (1990).

[13]B. H. Rabin, G. E. Korth, and R. L. Williamson, "Fabrication of Titanium Carbide–Alumina Composites by Combustion Synthesis and Subsequent Dynamic Consolidation," _J. Am. Ceram. Soc._, **73** [7] 2156–57 (1990).

[14]D. A. Hoke, M. A. Meyers, L. W. Meyer, and G. T. Gray III, "Reaction Synthesis/Dynamic Compaction of Titanium Diboride," _Metall. Trans._, **23A** [1] 77–86 (1992).

[15]J. LaSalvia, L. W. Meyer, D. A. Hoke, and M. A. Meyers; pp. 261–70 in _Shock-Wave and High-Strain-Rate Phenomena in Materials_. Edited by M. A. Meyers, L. E. Murr, and K. P. Staudhammer. Marcel Dekker, New York, 1992.

[16]M. A. Meyers, J. C. LaSalvia, D. A. Hoke, J. M. Jamet, and D. K. Kim; pp. 43–57 in Proceedings of the First International Conference on Advanced Synthesis of Engineered Materials (San Francisco, CA, August 31–September 2, 1992). ASM International, Metals Park, OH, 1993.

[17]J. C. LaSalvia, L. W. Meyer, and M. A. Meyers, "Densification of Reaction Synthesized Titanium Carbide by High-Velocity Forging," _J. Am. Ceram. Soc._, **75** [3] 592–602 (1992).

[18]J. C. LaSalvia, "Production of Dense Titanium Carbide by Combining Reaction Synthesis with Dynamic Compaction"; M.Sc. Thesis. University of California, San Diego, CA, 1990.

[19]D. A. Hoke, "A Study on the Reaction Synthesis and Dynamic Compaction of Titanium Diboride by a High Speed Forging Technique"; M.Sc. Thesis. University of California, San Diego, CA, 1991.

[20]J.-M. Jamet, "Study of the TiB_2–Al_2O_3 Composite Produced by Reaction Synthesis Followed by Dynamic or Quasi-Static Compaction"; M.Sc. Thesis. University of California, San Diego, CA, 1992.

[21]S. D. Dunmead, Z. A. Munir, and J. B. Holt, "Temperature Profile Analysis in Combustion Synthesis: II, Experimental Observations," _J. Am. Ceram. Soc._, **75** [1] 180–88 (1992).

[22]T. Kottke, L. J. Kecskes, and A. Niiler, "Control of Titanium Diboride SHS Reactions by Inert Dilutions and Mechanical Restraint," Report No. BRL-MR-3793, Ballistic Research Laboratory, U.S. Army Laboratory Command, Aberdeen Proving Ground, Maryland, December 1989, pp. 1–20.

[23]I. Barin; in _Thermochemical Data of Pure Substances_, Part I. VCH Publishers, New York, 1989.

[24]J. R. Ramberg and W. S. Williams, "High Temperature Deformation of Titanium Diboride," _J. Mater. Sci._, **22**, 1815–26 (1987).

[25]R. V. Raman, S. V. Rele, and M. J. Paskowitz, "_In-Situ_ Synthesis and Rapid Consolidation of Fully Dense $MOSi_2$," _J. Met._, **45** [1] 54–55 (1993).

[26]R. J. Green, "A Plasticity Theory for Porous Solids," _Int. J. Mech. Sci._, **14**, 215–24 (1972).

[27]M. Carrol and A. C. Holt, "Suggested Modification of the P-α Model for Porous Materials," _J. Appl. Phys._, **43** [2] 759–61 (1972).

[28]L. Banks-Sills and B. Budiansky, "On Void Collapse in Viscous Solids," _Mech. Mater._, **1**, 209–18 (1982).

[29]A. S. Helle, K. E. Easterling, and M. F. Ashby, "Hot-Isostatic Pressing Diagrams: New Developments," _Acta Metall._, **33** [12] 2163–74 (1985).

[30]M. Oyane, M. Omura, T. Tabata, and T. Hisatsune, "An Upper Bound Approach on Yield Surfaces of Porous Materials," _Ing.-Arch._, **59**, 267–73 (1989).

[31]P. M. McMeeking and L. T. Kuhn, "A Diffusional Creep Law for Powder Compacts," _Acta Metall._, **40** [5] 961–69 (1991).

[32]N. A. Fleck, L. T. Kuhn, and R. M. McMeeking, "Yielding of Metal Powder Bonded by Isolated Contacts," _J. Mech. Phys. Solids_, **40** [5] 1139–62 (1990).

[33]H. A. Kuhn and C. L. Downey, "Deformation Characteristics and Plasticity Theory of Sintered Powder Materials," _Int. J. Powder Met._, **7**, 15–25 (1971).

[34]S. M. Doraivelu, H. L. Gegel, J. S. Gunasekera, J. C. Malas, J. T. Morgan, and J. F. Thomas, Jr., "A New Yield Function for Compressible P/M Materials," _Int. J. Mech. Sci._, **26**, 527–35 (1984). ☐